Improved conductivity of aluminum-doped ZnO : the effect of hydrogen diffusion from a hydrogenated amorphous silicon capping layer

AIP | Journal of Applied Physics

Improved conductivity of aluminum-doped ZnO: The effect of hydrogen diffusion from a hydrogenated amorphous silicon capping layer

M. V. Ponomarev, K. Sharma, M. A. Verheijen, M. C. M. van de Sanden, and M. Creatore

Citation: J. Appl. Phys. **111**, 063715 (2012); doi: 10.1063/1.3692439
View online: http://dx.doi.org/10.1063/1.3692439
View Table of Contents: http://jap.aip.org/resource/1/JAPIAU/v111/i6
Published by the American Institute of Physics.

Improved conductivity of aluminum-doped ZnO: The effect of hydrogen diffusion from a hydrogenated amorphous silicon capping layer

M. V. Ponomarev,[1,a)] K. Sharma,[1] M. A. Verheijen,[1] M. C. M. van de Sanden,[1,2] and M. Creatore[1,b)]
[1]*Eindhoven University of Technology, Department of Applied Physics, P.O. Box 513, 5600 MB Eindhoven, The Netherlands*
[2]*DIFFER (Dutch Institute For Fundamental Energy Research), P.O. Box 1207, 3430 BE Nieuwegein, The Netherlands*

(Received 14 December 2011; accepted 9 February 2012; published online 27 March 2012)

Plasma-deposited aluminum-doped ZnO (ZnO:Al) demonstrated a resistivity gradient as function of the film thickness, extending up to about 600 nm. This gradient decreased sharply when the ZnO:Al was capped by a hydrogenated amorphous silicon layer (*a*-Si:H) and subsequently treated according to the solid phase crystallization (SPC) procedure at 600 °C. The resistivity reduced from $1.2 \cdot 10^{-1}$ to $2.6 \cdot 10^{-3}$ $\Omega \cdot$cm for a film thickness of 130 nm, while for thicker films the decrease in resistivity was less pronounced, i.e., a factor of 2 for a film thickness of 810 nm. While the carrier concentration was not affected, the mobility significantly increased from 7 to 30 $cm^2/V \cdot s$ for the thick ZnO:Al layers. This increase was ascribed to the passivation of grain boundary defects by hydrogen, which diffused from the *a*-Si:H toward the ZnO:Al during the SPC procedure. The passivation effect was more pronounced in thinner ZnO:Al layers, characterized by a smaller grain size, due to the presence of large grain boundaries. For thicker films with grain sizes up to 200–300 nm the mobility became progressively less affected by the presence of grain boundaries. Therefore, the hydrogen-induced improvement in conductivity was less significant for the thick ZnO:Al films. © *2012 American Institute of Physics*. [http://dx.doi.org/10.1063/1.3692439]

I. INTRODUCTION

Due to their wide bandgap, transparent conductive oxides (TCOs) exhibit a high transparency in the solar spectral range. Therefore, they are used as transparent electrodes in many applications, e.g., in flat panel displays,[1,2] for architectural and automotive glazing,[3] in solar thermal applications and in thin film solar cells (SC),[4–6] either silicon-[7,8] or non-silicon based, such as cadmium telluride,[9] and copper indium gallium diselenide.[10] Within the field of thin film silicon-based solar cells, poly-crystalline silicon (poly-Si) receives attention because it couples the potential for high conversion efficiency and lower production costs. One of the approaches toward poly-Si is plasma deposition of amorphous silicon followed by solid-phase crystallization (SPC),[11,12] which has delivered efficiencies up to 10%;[13,14] for example, CSG Solar[15] has achieved an efficiency of 10.4% by developing a 2.5 μm-thick poly-Si on glass, which was also confirmed by studies reported by Green *et al.*[15] In this case, the TCO can be applied as front contact and aluminum-doped zinc oxide (ZnO:Al) is often referred to as a valid alternative to, e.g., indium tin oxide. The ZnO is considered appealing due to the relatively low cost, high abundance, non-toxicity,[16,17] resistance to H_2 etching,[18,19] and, under specific conditions, surface texturing for light management/trapping.

This manuscript addresses the changes in the electrical properties which the ZnO:Al film undergoes upon SPC treatment of the hydrogenated amorphous silicon (*a*-Si:H) film deposited on top of the ZnO:Al. As already demonstrated by Lee *et al.*,[20] due to the application of a 300 nm thick *a*-Si capping layer on top of 700 nm sputtered ZnO:Al, a decrease in resistivity of the TCO layer was measured, i.e., from $(4.3 \pm 0.1) \cdot 10^{-4}$ to $(2.2 \pm 0.1) \cdot 10^{-4}$ $\Omega \cdot$cm after an SPC procedure up to 600 °C. The authors attributed this improvement to the increase in mobility of the charge carriers, which reached a value of 53 $cm^2/V \cdot s$. No further details were reported on the modification of the ZnO:Al layers upon annealing. The higher mobility was attributed to an improved crystallinity of the ZnO:Al layer, not further supported by any experimental evidence. Later, Ruske *et al.*[21] presented a more extended analysis of the above-mentioned results and reported an increase in mobility as well as in carrier concentration, reaching a value above 10^{20} cm^{-3}, upon annealing. The excellent results in terms of improved conductivity of the ZnO:Al layer upon annealing were attributed to hydrogen diffusion (i.e., as source of additional charge carriers) and to a decrease of defects at grain boundaries. Recently, the same research group improved the electrical properties of thermally degraded ZnO:Al films by means of a capping/annealing procedure.[22] They concluded that a transition from grain boundary scattering to ionized impurity scattering had occurred upon reduction of the defect density at the grain boundaries, after annealing of the films capped with *a*-Si:H.

In the present contribution, a 1 μm-thick *a*-Si:H layer, as typically used in poly-Si based solar cells, was deposited on ZnO:Al layers with a thickness in the range of 100–800 nm.

a)Electronic mail: m.ponomarev@tue.nl.
b)Electronic mail: m.creatore@tue.nl.

Both layers were synthesized by the expanding thermal plasma (ETP) technique.[11,23] In particular, following our previous studies[23] on highly conductive ($7 \cdot 10^{-4}\ \Omega \cdot$cm at a film thickness of 1300 nm) plasma-deposited ZnO:Al layers characterized by a strong gradient in resistivity as a function of the thickness, the present study focuses on the impact of the capping layer and the annealing on the gradient in resistivity of the ZnO:Al thickness series. Therefore, the electrical properties of the pristine ZnO:Al layer prior, as well as after the SPC treatment in the absence/presence of the *a*-Si:H layer, were determined. Moreover, the evaluation of the electrical properties is discussed as a function of the hydrogen diffusion profiles in the poly-Si/ZnO:Al stacks.

This paper is organized as follows: in Sec. II experimental details about sample preparation, post-deposition treatment and analysis techniques are provided. In Sec. III the experimental results on the correlation between the electrical and structural properties of the ZnO:Al films are presented and discussed. The gradient in resistivity of the as-deposited films, reduction of the gradient of capped, as well as a deterioration of the uncapped ZnO:Al films upon annealing are reported. Next to the changes in electrical properties, the hydrogen profile in the studied stacks was quantitatively followed by means of TOF-SIMS analysis. The obtained results, i.e. a massive reduction of the resistivity gradient of the capped ZnO:Al layer upon annealing and crystallization of the *a*-Si:H layer into poly-Si, was interpreted also in view of the ZnO:Al morphology development with thickness.

II. EXPERIMENTAL DETAILS

A remote plasma-enhanced chemical vapor deposition process, i.e., the ETP, was used for both depositions of ZnO:Al films on Corning 7059 glass and *a*-Si:H layers on top of ZnO:Al films. The plasma source was a cascaded arc, which generates a DC discharge between three cathodes and an anode plate at sub-atmospheric pressure (typically $P_{arc} = 0.3\text{–}0.5 \cdot 10^5$ Pa). Due to the pressure difference, the ionized argon expands into the low pressure deposition chamber (typically $P_{dep} = 30\text{–}200$ Pa) and dissociates the precursors injected through rings in the plasma jet: at 6.5 cm downstream from the plasma source oxygen was injected; further downstream at 30 cm from the plasma source pre-mixed diethylzinc (DEZ) and trimethylaluminum (TMA) were injected. ZnO:Al films have simultaneously been deposited on two glass (Corning 7059) and one mono-crystalline silicon substrates (<100> n-type Si), placed on a preheated substrate holder located at 50 cm from the plasma source.

In the present work, the experimental conditions were chosen to achieve highly conductive ZnO:Al with large surface roughness. In general, these conditions are appropriate for applications in solar cells, as earlier described.[18,23] As shown in Table I, the experimental parameters were kept constant, but the ZnO:Al thickness was in the range of 100 to 800 nm at the deposition rate of 1 nm/s.

On top of the glass substrates covered by ZnO:Al, 1000 nm-thick *a*-Si:H films were grown at 400 °C. In this case, the expanding thermal plasma was generated in an argon/hydrogen mixture. As a precursor for *a*-Si:H growth, silane (SiH_4) was used. It was fed into the plasma via an injection ring placed at 5 cm from the plasma source. More details were reported elsewhere.[24,25]

As a next step, an SPC process for 10 h at 600 °C in vacuum ($P = 10^{-4}$ Pa) was performed to fully crystallize *a*-Si:H. The heating rate was programmed as follows: 10 deg/min from room temperature to 400 °C followed by 1 deg/min in the range of 400–600 °C and 10 h at 600 °C. Afterwards, the power of the heater was switched off to let the samples cool down to room temperature.

The electrical properties were measured using a Jandel universal four-point probe with a cylindrical 25 mm probe head, following the approach of Ruske *et al.*[21] A VEECO Dektak 8 step-profiler was used to determine the thickness of the deposited films. Hall measurements were performed by means of a Phystech RH 2010 to determine the carrier concentration and mobility. A small preparation procedure was carried out to make good contacts with the capped ZnO:Al layer. On each corner of a 10×10 mm^2 poly-Si/ZnO:Al/glass samples ion beam etching of poly-Si layer was performed with a spot size of 2×1 mm^2. An argon-ion gun at 3000 eV and 3.85 μA was used for that, leading to an etch rate of $\sim$0.13 nm/s.

Surface morphology characterization was performed on an NT-MDT Solver P47 atomic force microscope (AFM) in a semi-contact mode with a scan size of $2 \times 2\ \mu$m^2. In addition, cross-sectional transmission electron microscopy (TEM) (FEI Tecnai F30ST transmission electron microscope operated at 300 kV) and scanning electron microscopy (SEM) (Jeol JSM-7500 FA) analyses were used to visualize the ZnO:Al grain development.

Rutherford backscattering spectroscopy (RBS) was employed to obtain quantitative information about the composition of the ZnO:Al films. In particular, RBS was used to measure zinc, oxygen, and aluminum content in the ZnO:Al films, needed for the calibration of data provided by the time-of-flight secondary ion mass spectrometry (ToF-SIMS) measurements. Hydrogen content was measured by means of elastic recoil detection analysis (ERD). Both RBS and ERD measurements were performed using 2 MeV He^+ ions produced by an HVE 3.5 MV singletron. In addition, the hydrogen concentration in *a*-Si:H films on c-Si substrate was calculated from the 640 cm^{-1} wagging mode in the spectra obtained by the Fourier transform infrared (FTIR) technique (Bruker Tensor 27), as described elsewhere.[26,27]

TABLE I. Summary of the experimental settings. Type of film and varied experimental conditions are indicated.

Type of film	G_{Ar}, sccm	G_{H2}, sccm	I_{Arc}, A	$P_{Arc} \times 10^5$, Pa	P_{Dep}, Pa	G_{DEZ}, g/h	G_{TMA}, g/h	G_{O2}, sccm	G_{SiH4}, sccm	T_{sub}, °C	Thickness, nm
ZnO:Al	1000	–	50	0.41	170	3.5	0.2	100	–	200	100–800
a-Si:H	3300	600	45	0.32	15	–	–	–	600	400	1000

The ToF-SIMS analysis on the ZnO:Al capped with SPC *a*-Si:H was performed to determine the elemental composition as a function of depth by means of a IONTOF TOF-SIMS IV instrument, using 25 keV Bi^+ ions from a 3-lens in both positive and negative modes. By calibrating these measurements with results determined from the ERD measurements, the hydrogen concentration in poly-Si on ZnO:Al was determined.

X-ray diffraction (XRD) measurements combined with *in situ* annealing at 600 °C were performed on a Philips MPD Control PW3710 X-Ray diffractometer to study the crystallization behavior of *a*-Si:H in more detail.

III. RESULTS

The resistivity trends as a function of the thickness for the as-deposited and annealed ZnO:Al films in the absence/presence of a capping layer are shown in Fig. 1(a). In agreement with the previous work,[23] a gradient in resistivity as function of the thickness was observed for the as-deposited ZnO:Al layers (Fig. 1(a), square symbol). This result was attributed to structural changes occurring during the growth of the poly-crystalline ZnO:Al layer, namely, a pyramid-like growth development of the ZnO:Al grains.[23] This type of growth is characterized by an increase in grain size and, consequently, a reduction in the density of grain boundaries and charge trapping centers, leading to an enhanced mobility.[23] At the same time, the ZnO:Al, which was capped with *a*-Si:H and had received an SPC treatment (Fig. 1(a), circle symbol), exhibited a decrease in resistivity. In particular, the effect had a major impact on the thinner films, leading to a significant decrease of resistivity and a suppression of the resistivity gradient. On the contrary, annealing the uncapped ZnO:Al at SPC conditions in vacuum deteriorated its electrical properties (Fig. 1(a), triangle symbol), in agreement with Minami *et al.*,[28] and the effect was more pronounced for larger ZnO:Al thickness values.

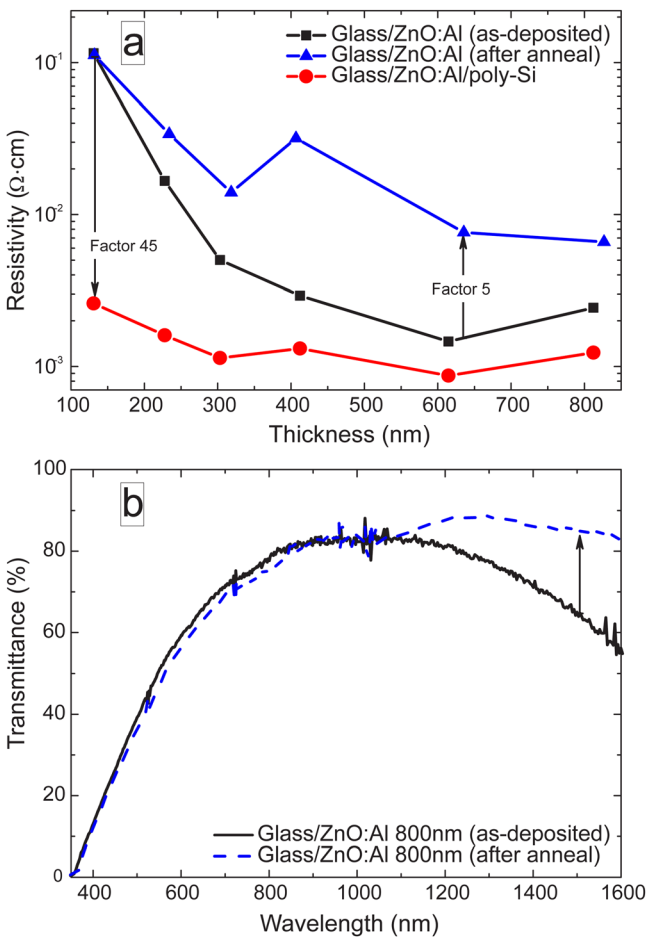

FIG. 1. (Color online) (a) Changes in resistivity of the ZnO:Al layer as function of the thickness upon anneal in the absence/presence of a capping *a*-Si:H layer; (b) Changes in the straight-through transmittance for the 810 nm thick ZnO:Al film before and after SPC treatment.

The deterioration of the electrical properties of the uncapped ZnO:Al can be related to the oxygen present at the grain boundaries. One possible explanation is the formation of Al_2O_3 at the grain boundaries, based on the presence of residual oxygen during vacuum annealing. This oxidation is thermodynamically favored due to its high formation enthalpy.[4] The increase in resistivity clearly correlates with measurements of the VIS-NIR (650–1700 nm) transmittance of the uncapped ZnO:Al films, which significantly increased after annealing under SPC conditions, as shown in Fig. 1(b) for the 810 nm thick ZnO:Al sample. The effect is in agreement with observations of Lee *et al.*[20] and suggests that the absorption by free charge carriers in the near-infrared is considerably reduced. Therefore, it can be concluded that a decrease in doping efficiency can be caused by the formation of Al_2O_3, which acts as neutral impurity scattering center.

Another reason for the deterioration effect observed in Fig. 1(a) is based on the considerations reported by Minami *et al.*:[28] oxygen chemisorbed at the grain boundaries can capture free electrons from the bulk of the grain, creating extrinsic interface states. There are several factors related to the grain boundaries that can reduce the mobility, namely, fairly high densities of interface states which trap free carriers from the bulk of the grains, scattering of free carriers induced by the inherent disorder and the presence of trapped charges.[29] According to the grain boundary carrier-trapping model,[30–32] oxygen adsorbed at the grain boundaries results in an additional interface charge, which gives rise to band-bending (the energy difference between the conduction band edge at the grain boundary and in the bulk of the grain) in the bulk of the grain and to the creation of potential energy barriers.[29] These grain boundary barriers hinder the motion of free carriers from one grain to another by scattering them back to the bulk of the grain, thereby their inter-grain mobility is reduced and overall the film resistivity increases.

Next to the study of the uncapped layers, the properties of ZnO:Al layers capped with *a*-Si:H were evaluated. As pointed out by Ruske *et al.*,[21] the improvement of the electrical properties of capped ZnO:Al was caused by the hydrogen available in the *a*-Si:H capping layer before the SPC procedure, although an additional source of hydrogen was present in their sample, i.e., a SiN_x:H layer between the glass substrate and the ZnO:Al layer.

On the basis of the FTIR analysis of the present experiments, the hydrogen concentration in the as-deposited *a*-Si:H was equal to $(3.6 \pm 0.3) \cdot 10^{21}$ at/cm^3. The ERD-measured

hydrogen concentration in the as-deposited ZnO:Al layer was $(2.7 \pm 0.3) \cdot 10^{20}$ at/cm^3, which is one order of magnitude lower than in *a*-Si:H. Therefore, during the SPC process of *a*-Si:H, it is expected that hydrogen diffuses into the ZnO:Al layer, as well escapes toward the ambient[33] (i.e., the oven). Within the ZnO:Al layer, hydrogen can reduce the grain boundary defects that limit the film conductivity. It also forms a strong bond with oxygen, providing a powerful driving force for its incorporation in the ZnO crystal.[34] According to Van de Walle,[34] hydrogen in ZnO appears exclusively in the positive charge state, i.e., it always acts as a donor causing an increase in carrier concentration. Therefore, it tends to reduce the energy barriers at the grain boundaries, thus being the main reason for the improved electrical properties,[35] in agreement with Ruske *et al.*[21] Other mechanisms, such as reduction of point defects and activation of the Al from Al-oxide phase[36,37] are also possible and should not be disregarded. For example, Kim *et al.*[37] showed activation of Al dopants through deoxidation of Al-oxides, after annealing ZnO:Al films at 900 °C for 3 mins.

However, as shown in Fig. 1(a), the hydrogen impact on the electrical properties is dependent on the thickness of the ZnO:Al film. For the 130 nm-thick ZnO:Al film, the resistivity improved by a factor 45 (to $2.6 \cdot 10^{-3}$ $\Omega \cdot$cm), while for the 810 nm-thick layer the improvement was only a factor of 2 (to $1.2 \cdot 10^{-3}$ $\Omega \cdot$cm). This is because of the large influence of the grain boundary states on the lateral film resistivity/mobility, as already concluded by Volintiru *et al.*[38] A similar effect was observed by Wimmer *et al.*[22] for 900 nm-thick ZnO:Al: capping and annealing of as-deposited film resulted in a factor of 2 improvement in resistivity ($\sim 2.4 \cdot 10^{-4}$ $\Omega \cdot$cm), while this latter was increasing by more than a factor of 100 for the thermally degraded films with the lowest carrier concentration and mobility.

The carrier concentration measured in the capped ZnO:Al was about $3 \cdot 10^{20}$ cm^{-3} and the mobility was around 30 cm^2/V $\cdot$ s for the 600 nm thick ZnO:Al layer and about the same value for the 200 nm thick film. The carrier concentration is in agreement with the value associated to the pristine ZnO:Al ($2 \cdot 10^{20}$ cm^{-3}) and the mobility significantly increased from the as-deposited state (7 cm^2/V $\cdot$ s at 600 nm). This result also points out that the grain boundaries are passivated by hydrogen. Moreover, it agrees well with the observations of Ruske *et al.*,[21] who reported a significant increase of the mobility. The same research group also showed a faster poly-crystalline silicon nuclei development on ZnO:Al films, as compared to SiN_x:H films,[39] in agreement with *in situ* crystallization study of this work (data not shown here). As inferred from *in situ* XRD measurements,[40] the formation of nuclei in the *a*-Si:H capping layer occurred already after 60 mins of annealing at 600 °C in the case of 810 nm-thick ZnO:Al, while, in the case of *a*-Si:H deposited on glass, the nucleation started after 180 mins.

To understand the effect of annealing in more detail, the in-depth hydrogen distribution was studied in the poly-Si/ZnO:Al stacks. In Fig. 2 ToF-SIMS depth profiles are presented for the ZnO:Al capped with SPC *a*-Si:H samples with 810 nm-thick (Fig. 2(a)) and 130 nm-thick (Fig. 2(b)) ZnO:Al. For simplicity, only the hydrogen, silicon, zinc oxide, and silicon dioxide profiles are shown. The Si signal intensity was constant and equal in both samples, pointing out similar properties of the poly-Si capping layer in both cases. The poly-Si/ZnO:Al and ZnO:Al/glass interfaces for both samples are for sake of simplicity defined by means of two vertical lines in Fig. 2. Due to the larger roughness of the 800 nm-thick ZnO:Al layer as compared to the 130 nm layer (r.m.s. values obtained from AFM measurements: 40 versus 15 nm, respectively), the poly-Si/ZnO:Al interface region is found to be broader for the thicker ZnO:Al layer. Therefore, it appeared earlier on the time scale of the ToF-SIMS analysis (Fig. 2(a)) as compared to the sample with a thinner ZnO:Al layer (Fig. 2(b)). At the same time, the hydrogen profiles are significantly different. In order to extract quantitative information, the hydrogen depth profiles were calibrated by means of the ERD analysis, and the results are shown on the right axis in Fig. 2. The hydrogen in the poly-Si on 130 nm-thick ZnO:Al is below the detection limit (i.e., $1–2 \cdot 10^{19}$ at/cm^3) almost through the whole poly-Si layer and abruptly rises just at the interface with the ZnO:Al film to 10^{21} at/cm^3. For the sample with 810 nm-thick ZnO:Al the hydrogen concentration increases gradually from the poly-Si layer to 10^{21} at/cm^3 at the interface

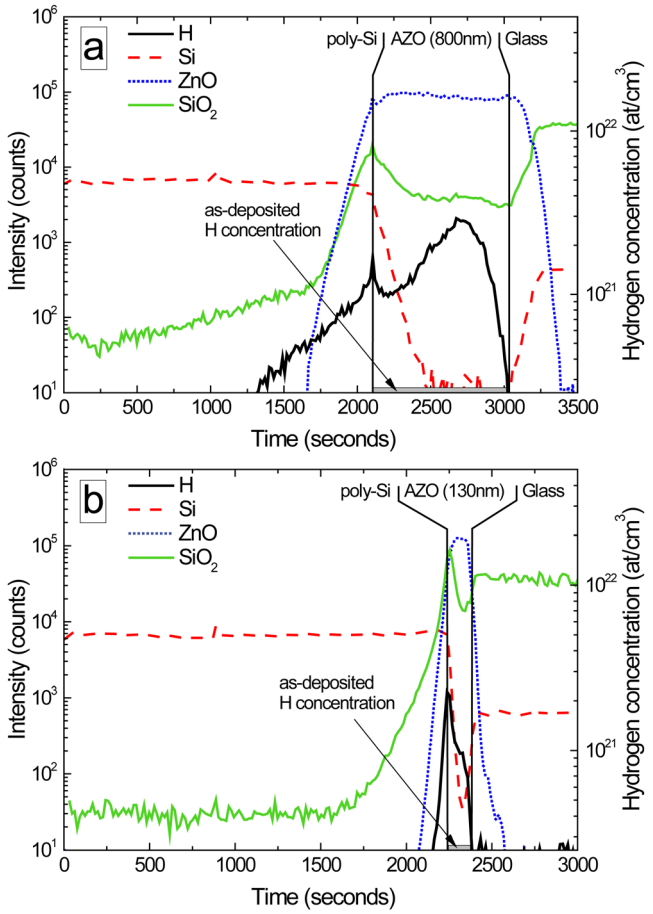

FIG. 2. (Color online) ToF-SIMS profiles of poly-Si/ZnO:Al/glass samples: (a) $d_{ZnO:Al} = 810$ nm; (b) $d_{ZnO:Al} = 130$ nm. The local maximum in the hydrogen profile at the poly-Si/ZnO:Al interface is accompanied by an enhancement in count rate for several other signals, i.e., F-, S- (both are not shown here), and SiO_2. This result could be morphology-related (i.e., the surface roughness of the ZnO:Al layer can induce an artifact in the ToF-SIMS profile, especially in the case of the thickest sample) and possibly dependent on an intermixing effect during the ToF-SIMS analysis.

with the ZnO:Al layer and up to $3 \cdot 10^{21}$ at/cm^3 halfway the ZnO:Al layer thickness. The conclusion is that for both ZnO:Al films the hydrogen concentration is significantly higher when compared to the one in the pristine ZnO:Al film (also shown in Fig. 2). This implies that hydrogen diffused from the *a*-Si:H layer into the ZnO:Al and was effectively stored after the SPC process.

The reason why the hydrogen concentration is higher for the thicker ZnO:Al film may be related to the layer structure providing a larger grain-boundary surface available for atomic hydrogen to be trapped and stored. This hypothesis is supported by the fact that the ZnO:Al layers were grown under the same experimental conditions and presented the same doping concentration (0.37% Al in 130 nm ZnO:Al and 0.36% Al in 810 nm ZnO:Al, as measured by ToF-SIMS and calibrated by means of the RBS results). Therefore, cross-sectional TEM analyses were carried out to get an insight into the ZnO:Al growth development (Fig. 3, cross-sectional high angle annular dark field-scanning transmission electron microscopy (HAADF STEM)).

At early growth stages, below 100 nm of film thickness, there was a layer of very densely packed crystallites extending over few tens of nm. During film growth, some grain orientations were suppressed, while others continued to develop either vertically and/or laterally. As observed in Fig. 3, this growth was accompanied by the inclusion of large voids extending up to few hundred nanometers in height developing at 100–600 nm from the substrate surface. Then, the developed grains coalesced at 600–700 nm height and formed a dense matrix with no further inclusion of voids. This is important for the lateral current propagation, especially within thinner layers of ZnO:Al, where the total area of the grain boundaries is higher due to the smaller crystal size. If defects at the grain boundaries are not passivated, the grain boundary scattering together with the presence of voids can significantly limit the lateral conductivity. For the ZnO:Al films grown under these conditions, the carrier concentration was about $2 \cdot 10^{20}$ cm^{-3}, which is considered to be a rather high doping level. According to the grain boundary carrier-trapping model,[29–31] the charge carriers can be trapped at the grain boundaries, producing a charged grain boundary surrounded by a space-charge region. The resistivity of this space-charge region can limit the conductivity of the sample. With an increase in doping concentration the barrier height decreases and the space-charge region gets narrower. Because there is an exponential dependence of the grain boundary resistivity on the barrier height,[30] this resistivity will decrease faster than the one of the grains. Therefore, at heavy doping levels, grain boundaries do not limit the conductivity anymore,[41] so the mobility becomes independent from the grain size. However, from Fig. 1(a) the resistivity of the as-deposited samples is thickness-dependent, or, since the grain size is increasing with thickness, grain size-dependent. Thus, the potential at the grain boundaries has to be considered, as influencing the mobility of the charge carriers.

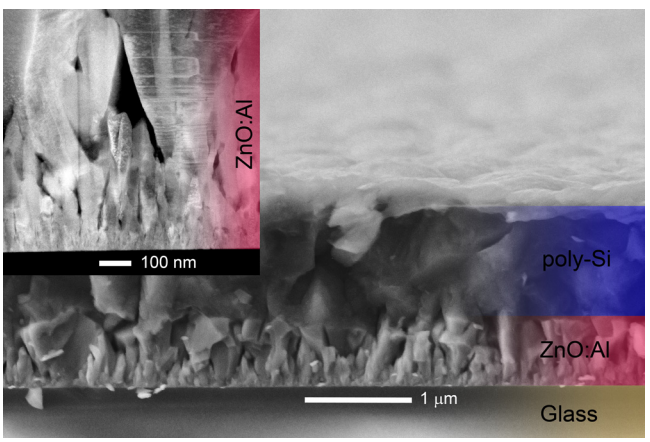

FIG. 3. (Color online) Scanning electron microscopy image of poly-Si (1000 nm) on ZnO:Al (810 nm)/glass. Inset: Cross-sectional HAADF-STEM image of ZnO:Al film on glass. Dark areas represent voids in the layer.

As extensively discussed in our previously published work,[23] the lateral conductivity is effectively limited by the relatively high grain boundary density at the early stages of ZnO:Al growth. With an increase in film thickness, the lateral conductivity becomes gradually less affected by the grain boundary scattering and more by the ionized impurity scattering phenomena, as the grains develop in size. At intermediate thicknesses, i.e., where large voids develop, the percolation path for the charge carriers becomes longer and the scattering mechanisms in the bulk ZnO:Al become relevant. In agreement with Wimmer *et al.*,[22] the impact of hydrogen in improving the ZnO:Al conductivity is attributed to the reduction of the defect density at the grain boundaries of the ZnO:Al layer. This effect is larger in the case of low ZnO:Al film thickness, because the mobility is limited here by the small grain size and, thus, by the grain boundaries. In case of 700–800 nm-thick ZnO:Al films the passivation of grain boundaries still occurs, under the reasonable assumption that the grain boundary defect density is independent from the layer thickness. However, due to the developed larger grain size (200–300 nm), the passivation has a less pronounced effect on the resistivity, as shown in Fig. 1(a). It can be expected that the limited improvement in conductivity for large ZnO:Al thickness values observed in Fig. 1(a) is also caused by hydrogen diffusing in the grains, providing additional doping[33,34,42,43] and, thereby, promoting a stronger contribution of the ionized impurity scattering. It has been recently demonstrated[22] that upon annealing of the capped ZnO:Al films the scattering mechanism shifts from grain boundary scattering to ionized impurity scattering.

Furthermore, the local maximum observed in the hydrogen profile in Fig. 2(a) at 2700 s of the ToF-SIMS analysis can be attributed to the presence of the voids as indicated by the HAADF STEM image in Fig. 3. The maximum corresponds to a height of about 300 nm of ZnO:Al, where the large pores start to appear allowing atomic hydrogen to readily distribute within the network of voids and be trapped at the large grain boundary surface available.

The structural development of ZnO:Al can also explain the behavior of the uncapped films, where annealing mostly affected films from intermediate to larger thicknesses (Fig. 1(a), triangles). As shown in the HAADF STEM image inset in Fig. 3, the grain size is quite large at the intermediate thickness (300–600 nm), but there are also large voids at that thickness

which allow for easier oxygen diffusion within the ZnO:Al film, adsorbing at the grain boundaries. There, it increases the grain boundary potential for the charge carriers and, in combination with the presence of voids, it induces a longer percolation path for the charge carriers. Therefore, the resistivity at intermediate thicknesses is more affected by annealing. With the further increase in film thickness (600–800 nm), when there are no voids and the grain boundary surface area is reduced, the degradation effect on electrical properties is limited.

IV. CONCLUSIONS

The application of a capping layer of *a*-Si:H on ZnO:Al layers followed by SPC treatment allows for a strong reduction of the gradient in resistivity as function of the thickness of the ZnO:Al layer underneath. A major improvement of the electrical properties was observed in the thinner films: for the 130 nm-thick film, the resistivity is reduced by a factor 45 down to $2.6 \cdot 10^{-3}$ $\Omega \cdot$cm. For the thicker films the effect was less pronounced and mainly caused by the increased mobility of the charge carriers, e.g., from 7 $cm^2/V \cdot s$ to 30 $cm^2/V \cdot s$ for the 600 nm-thick ZnO:Al.

The improvement of the electrical properties was attributed to the passivation of the grain boundaries by hydrogen diffused from the *a*-Si:H capping layer. Although a higher concentration of hydrogen was measured in the stack poly-Si/ZnO:Al layers in the case of the thick ZnO:Al film, the passivation of grain boundaries was found to have a larger impact in the case of thin ZnO:Al films. In this case, charge carrier mobility is strongly limited by the rather small grain size and, therefore, grain boundary effects. On the contrary, at large ZnO:Al thickness values, characterized by a larger grain size and compact structure, the mobility of the charge carriers was less affected by the grain boundaries. Therefore, the passivation had a significantly smaller effect on the resistivity of the thick films. In the case of uncapped ZnO:Al films the annealing mainly deteriorated the areas with the developed network of voids.

In conclusion, highly conductive and thinner front contacts for thin film poly-Si based PV can be obtained upon SPC processing of the *a*-Si:H layer. Hydrogen provides efficient passivation of the trapping states at the grain boundaries, which improves the electrical properties significantly and, if stable in time, provides a novel approach to improve the electrical properties of thin ZnO:Al films.

ACKNOWLEDGMENTS

The authors would like to thank J.A. Treur, R.H.J. Vervuurt, B.W.H. van de Loo for their assistance in samples preparation and analysis. Also, the authors acknowledge Dr. T. Fernandez Landaluce (TU Eindhoven) for sputtering the poly-Si capping layers during preparation for Hall measurements, ir. J.H.M. Snijders (Philips Innovation Services) for ToF-SIMS measurements, and M.J.F. van de Sande and J.J.A. Zeebregts, M.Sc. (TU Eindhoven) for the extensive technical assistance. This work has been supported within the IRTES project (project number 10007870) by Agentschap NL.

[1]Y. Li, G. S. Tompa, S. Liang, C. Gorla, Y. Lu, and J. Doyle, J. Vac. Sci. Technol. A: Vacuum, Surfaces and Films **15**(3), 1063 (1997).
[2]C. Agashe, O. Kluth, G. Schope, H. Siekmann, J. Hupkes, and B. Rech, Thin Solid Films **442**(1–2), 167 (2003).
[3]C. G. Granqvist, Solar Energy Mater. Solar Cells **91**(17), 1529 (2007).
[4]S. Jager, B. Szyszka, J. Szczyrbowski, and G. Brauer, Surf. Coat.Technol. **98**(1–3), 1304 (1998).
[5]B. Rech and H. Wagner, Appl.Phys. A: Mater. Sci. Process. **69**(2), 155 (1999).
[6]A. Nemeth, C. Major, M. Fried, Z. Labadi, and I. Barsony, Thin Solid Films **516**(20), 7016 (2008).
[7]W. M. M. Kessels, M. C. M. van de Sanden, and D. C. Schram, J. Vac. Sci. Technol. A: Vacuum, Surfaces, and Films **18**(5), 2153 (2000).
[8]O. Kluth, G. Schope, J. Hupkes, C. Agashe, J. Muller, and B. Rech, Thin Solid Films **442**(1–2), 80 (2003).
[9]M. Hadrich, C. Kraft, C. Loffler, H. Metzner, U. Reislohner, and W. Witthuhn, Thin Solid Films **517**(7), 2282 (2009).
[10]N. Naghavi, D. Abou-Ras, N. Allsop, N. Barreau, S. Bucheler, A. Ennaoui, C. H. Fischer, C. Guillen, D. Hariskos, J. Herrero, R. Klenk, K. Kushiya, D. Lincot, R. Menner, T. Nakada, C. Platzer-Bjorkman, S. Spiering, A. N. Tiwari, and T. Torndahl, Prog. Photo.: Res. Appl. **18**(6), 411 (2010).
[11]A. Illiberi, K. Sharma, M. Creatore, and M. C. M. van de Sanden, Mater. Lett. **63**(21), 1817 (2009).
[12]K. Sharma, A. Branca, A. Illiberi, F. D. Tichelaar, M. Creatore, and M. C. M. van de Sanden, Adv. Energy Mater. **1**(3), 401 (2011).
[13]T. Matsuyama, K. Wakisaka, M. Kameda, M. Tanaka, T. Matsuoka, S. Tsuda, S. Nakano, Y. Kishi, and Y. Kuwano, Jpn. J. Appl. Phys. Part 1-Regular Papers Short Notes & Review Papers **29**(11), 2327 (1990).
[14]T. Matsuyama, N. Terada, T. Baba, T. Sawada, S. Tsuge, K. Wakisaka, and S. Tsuda, J. Non-Cryst. Sol. **198–200**(Part 2), 940 (1996).
[15]M. A. Green, P. A. Basore, N. Chang, D. Clugston, R. Egan, R. Evans, D. Hogg, S. Jarnason, M. Keevers, P. Lasswell, J. O'Sullivan, U. Schubert, A. Turner, S. R. Wenham, and T. Young, Solar Energy **77**(6), 857 (2004).
[16]K. Ellmer, F. Kudella, R. Mientus, R. Schieck, and S. Fiechter, Thin Solid Films **247**(1), 15 (1994).
[17]J. Muller, B. Rech, J. Springer, and M. Vanecek, Solar Energy **77**(6), 917 (2004).
[18]J. Loffler, R. Groenen, J. L. Linden, M. C. M. van de Sanden, and R. E. I. Schropp, Thin Solid Films **392**(2), 315 (2001).
[19]R. Groenen, M. Creatore, and M. C. M. van de Sanden, Appl. Surf. Sci. **241**(3–4), 321 (2005).
[20]K. Y. Lee, C. Becker, M. Muske, F. Ruske, S. Gall, B. Rech, M. Berginski, and J. Hupkes, Appl. Phys. Lett. **91**(24), 241911 (2007).
[21]F. Ruske, M. Roczen, K. Lee, M. Wimmer, S. Gall, J. Hupkes, D. Hrunski, and B. Rech, J. Appl. Phys. **107**(1), 013708–1 (2010).
[22]M. Wimmer, F. Ruske, S. Scherf, and B. Rech, Thin Solid Films **520**, 4203 (2012).
[23]I. Volintiru, M. Creatore, B. J. Kniknie, C. I. M. A. Spee, and M. C. M. van de Sanden, J. Appl. Phys. **102**(4), 043709-1 (2007).
[24]M. C. M. van de Sanden, R. J. Severens, W. M. M. Kessels, R. F. G. Meulenbroeks, and D. C. Schram, J. Appl. Phys. **84**(5), 2426 (1998).
[25]W. M. M. Kessels, R. J. Severens, A. H. M. Smets, B. A. Korevaar, G. J. Adriaenssens, D. C. Schram, and M. C. M. van de Sanden, J. Appl. Phys. **89**(4), 2404 (2001).
[26]R. J. Severens, G. J. H. Brussaard, M. C. M. van de Sanden, and D. C. Schram, Appl. Phys. Lett. **67**(4), 491 (1995).
[27]A. H. M. Smets, W. M. M. Kessels, and M. C. M. van de Sanden, Appl. Phys. Lett. **82**(10), 1547 (2003).
[28]T. Minami, T. Miyata, and T. Yamamoto, J. Vac. Sci. Technol. A-Vacuum Surfaces and Films **17**(4), 1822 (1999).
[29]J. W. Orton and M. J. Powell, Rep. Prog. Phys. **43**(11), 1263 (1980).
[30]T. I. Kamins, J. Appl. Phys. **42**(11), 4357 (1971).
[31]J. Y. W. Seto, J. Appl. Phys. **46**(12), 5247 (1975).
[32]G. Baccarani, B. Ricco, and G. Spadini, J. Appl. Phys. **49**(11), 5565 (1978).
[33]N. H. Nickel, Phys. Rev. B **73**(19), 195204-1 (2006).
[34]C. G. Van de Walle, Phys. Rev. Lett. **85**(5), 1012 (2000).
[35]B. Y. Oh, M. C. Jeong, D. S. Kim, W. Lee, and J. M. Myoung, J. Cryst. Growth **281**(2–4), 475 (2005).
[36]N. Ohta, D. Ohba, S. Sato, Z. Tang, H. Shimizu, and H. Shirai, Thin Solid Films **519**(20), 6920 (2011).

[37]K. K. Kim, H. Tampo, J. O. Song, T. Y. Seong, S. J. Park, J. M. Lee, S. W. Kim, S. Fujita, and S. Niki, Jpn. J. Appl. Phys. Part 1-Regular Papers Brief Communications & Review Papers **44**(7A), 4776 (2005).
[38]I. Volintiru, M. Creatore, and M. C. M. van de Sanden, J. Appl. Phys. **103**(3), 033704-1 (2008).
[39]T. Sontheimer, C. Becker, U. Bloeck, S. Gall, and B. Rech, Appl. Phys. Lett. **95**(10), 101902-1 (2009).
[40]K. Sharma, M. A. Verheijen, M. C. M. van de Sanden, and M. Creatore, J. Appl. Phys. **111**, 033508 (2012).
[41]J. Steinhauser, S. Fay, N. Oliveira, E. Vallat-Sauvain, and C. Ballif, Appl. Phys. Lett. **90**(14), 142107-1 (2007).
[42]J. H. Lee, Curr. Appl. Phys. **10**(3), S515 (2010).
[43]B. Y. Oh, M. C. Jeong, and J. M. Myoung, Appl. Surf. Sci. **253**(17), 7157 (2007).